SPE/ATW

Collapse Behavior of Casings: Measurement Techniques, Numerical Analyses and Full Scale Testing

A.P. Assanelli, R.G. Toscano, D.H. Johnson and E.N. Dvorkin, Center for Industrial Research/FUDETEC

This paper was prepared for presentation at the 1998 SPE/ATW Risk Based Design of Well Casing and Tubing, held in The Woodlands, Texas, 7–8 May 1998.

Abstract

The production of steel OCTG products with guaranteed external collapse pressure (high collapse casing) requires the implementation of an accurate process control. To develop that process control it is necessary to investigate how different parameters affect the external collapse pressure of pipes. Two dimensional finite element models provide an useful tool for performing the "first approach" parametric studies; however a bidimensional representation of the tube geometry (as used in many analytical and semi-empirical formulas) is not enough for determining the external collapse pressure of casings. We use three dimensional models to further investigate the effects of the casing geometry on its external collapse pressure. To acquire the data that dscribes the geometry of casing samples, we have developed an imperfections measurement system following previous developments by Yeh and Kyriakides. We also present finite element models of OCTG connections which are used as a tool for the evaluation of connections collapse pressure.

Introduction

The external collapse pressure of very thin steel pipes is governed by classical elastic buckling formulas[1,2]; however, for thicker pipes more involved elasto-plastic considerations have to be taken into account. There are many factors that have some degree of influence on the external pressure that produce the collapse of a steel pipe, among them[3-9]:

- The relation outside diameter/thickness (D/t).
- The yield stress of the pipe steel (σ_y).
- The shape of the pipe sections (outside diameter shape and thickness distribution).
- The residual stresses locked in the pipe steel.
- The work - hardening of the pipe steel.
- The localized imperfections introduced either in the pipes production, in the pipes handling or due to localized wear.

In this paper we discuss the experimental techniques and the hierarchy of finite element models that we have developed to study the collapse behavior of seamless steel pipes.

We first comment on our facilities for performing external pressure collapse tests and we also present an imperfection measuring system (IMS) that we have implemented at our laboratory based on devices presented by Yeh et al[10] and Arbocz et al[11,12].

Then we describe some simple 2D finite element models that we have developed as a first approach for the simulation of the external pressure collapse test. We compare the results that these 2D models provide with the experimental results obtained at our laboratory; the comparison demonstrates that a 2D geometrical characterization of the pipes does not contain enough information to quantitatively assess on their collapse strength.

The pipe shape imperfections and the wall thickness normally change along the pipe length; also localized imperfections can be found in the pipes. In Section 4 we present the 3D finite element models that we have developed to overcome the limitations of the simpler 2D models. The 3D model predictions have been qualified via experimental testing at our laboratory. The geometrical information on the tested samples has been acquired using our imperfections measuring system and has been used as input data for our 3D finite element models.

Experimental Procedures

The core of any high collapse development is the "collapse test", basically described in API *Bull.* 5C3[13], Sect.2, but with a modified length to diameter ratio (L/D). Along with the physical testing, accurate measurements must be performed, to document the test itself as well as to feed mathematical models. A database is then necessary in order to organize the information obtained from the tests.

External pressure collapse tests. The collapse chamber used in this investigation has been designed along the basic design of API Bull. 5C3, with the important modification of the L/D

ratio. A summary of its features includes:

- The experimental set-up does not impose any axial restrain on the pipes.
- The length of the sample being tested fulfills in all cases the relation[6]: $L/D \geq 10$.
- The collapse of the samples is detected by a drop in the pressure of the water used to pressurize them.
- The chamber can be moved to a testing frame to add axial load to the sample.
- Samples with connections can be tested, with or without axial loads.

Imperfections measuring system. All samples are measured following standard practices. Ovality and eccentricity are measured and recorded at a specified number of locations. Longitudinal and transversal yield stresses, as well as residual stresses are also measured for each sample. In addition, for selected pipes, in-depth pipe outside diameter (OD) and thickness mappings are performed. This procedure is based on the one presented by Yeh and Kyriakides, among others[10-12].

Mapping of the samples geometry. To map the external surface, the sample is rotated in a lathe and at regular intervals of time, axial and angular position, are sent to the acquisition system (**Fig. 1**). The position of the pipe surface is measured via a Linear Variable Displacement Transducer (LVDT). A rotary encoder placed in the rotation axis provides the angular position information. In Appendix A we show the algorithm (**Fig. 2**) we have developed to transform the acquired data into the actual mapping of the pipe surface and its Fourier series decomposition (**Figs. 3 and 4**). It must be noted that standard ovality measurements are "blind" to mode shapes of odd order (such as a "cloverleaf" shape, order 3).

As an example, for a 9 5/8in. sample 2900 mm are mapped, at an average rate of approximately 96000 points per meter. The LVDT tip follows a helical path, with a pitch of 3.7 mm. It is assumed that this pitch is small enough to consider each turn as representative of one section. In the present setup of the device, the thickness is measured manually at 272 locations, using an ultrasonic gauge (**Fig. 5**). An enhancement of the device is planned, which will allow to measure the wall thickness on-line with the outside diameter.

Residual stress test. Residual stresses are measured with the slit ring method. A detailed analysis using 2D and 3D finite element models of this test is included elsewhere[14].

Full scale test database. The information of the full scale test is stored in a database. More than 100 fields are recorded for each test. Previous experience with smaller databases showed that if an accurate process control should take any benefit from it, the number of fields could not be reduced. The recorded fields include:

- Description fields (14): Nominal OD, grade, wall thickness, test date, etc.
- Geometric measurement fields (36): Measured ODs, thickness, etc.
- Mechanical Properties (14): yield strength, ultimate strength, collapse load, etc.
- Process parameters (11): information on straightening, heat treatment, etc.
- Calculated fields (31): Average ODs, average wall thickness, etc.

Test results that require direct measurement plus additional calculations (i.e.: residual stress test, ovality, eccentricity, etc.), are stored as calculated fields, with the only exception of ASTM tensile tests.

Pipes measured with the IMS are also registered and measured independently in the standard way. This latter information is recorded in the database.

Finite Element Procedures

The finite element method is the basic numerical tool we use to perform the analyses. Two and three dimensional models are currently used for collapse analyses. In all cases we use finite element models[15-20] that satisfy the reliability criteria outlined in Appendix B and that incorporate geometrical nonlinearities due to large displacements/rotations[21], material nonlinearity due to the elasto-plastic behavior (von Mises associated plasticity[21] is used) and follower (hydrostatic) loads.

Bidimensional finite element models. Bidimensional (2D) finite element models have been implemented to simulate the behavior of ideal "long specimens" in the external pressure collapse test[9]. A discussion on different bidimensional characterizations (plane stress, plane strain) is given elsewere[14]. As it will be shown later, the comparison between models and results from the database demonstrates that a 2D geometrical characterization of the pipes does not contain enough information to accurately assess on their collapse strength. However, 2D models can provide useful information on the trends of the external collapse pressure value when some parameters -such as residual stresses, shape imperfections, etc.- are changed.

Parametric analyses. Using 2D finite element models, we develop in this Section a parametric study aimed at the analysis of the effect, on the pipe collapse pressure, of the following parameters:

- Ovality [$O_V = (D_{max} - D_{min})/D_{average}$]
- Eccentricity [$\varepsilon = (t_{max} - t_{min})/t_{average}$]
- Residual stresses (σ_R)

In the present analyses the ovality is considered to be concentrated in the shape corresponding to the first elastic buckling mode and the eccentricity is modeled considering non-coincident, perfectly circular (or oval) OD and ID centers. In all cases a 9 5/8in. pipe with 110 ksi yield stress is considered. The wall thickness is varied for this analysis from thin wall (elastic collapse) to thick wall (plastic collapse).

In **Fig. 6** we plot the results of our parametric study, normalized with the collapse pressure calculated according to API standards[13]. It is obvious from these results that the main influence on the external collapse pressure comes from the ovality and from the residual stresses; however, the effect of

the residual stresses diminishes when the ratio (D/t) evolves from the plastic collapse range to the elastic collapse range. The eccentricity effect, in the case of the external collapse test with neither axial nor bending loads, is minor.

The effect of the hardening characteristic of the base material is found to be dependent on the definition of the yield point. If an offset yield is adopted, the influence of the hardening modulus is negligible for typical values[14].

Comparison with results from the database. The above results are coincident with most of what is already known in collapse of pipes[6-9]. However, even if the results have an important qualitative significance, a case by case comparison shows quantitative differences. **Fig. 7** shows the relation between results from bidimensional models and full scale tests for 32 cases from our database. A large spread is observed, and the average shows that 2D model results are conservative. Some reasons for this behavior are:

- Only one ovality is not fully representative of the sample geometry (in our case the middle section ovality).
- In developing the 2D models the measured ovality is entirely assigned to the first elastic buckling mode and this conservative approach partially accounts for the fact that the numerical values are lower than the actual ones.
- The collapse chamber imposes on the samples unilateral radial restraints at both ends[6], these restraints are not described by the 2D models; the difference between the numerical and actual boundary conditions also partially accounts for the fact that the numerical values are in general lower than the actual ones.

Three dimensional finite element models. A coupling of the imperfections measuring device along with full three dimensional finite element models of the collapse test was implemented, in order to resolve the above mentioned discrepancies.

The slenderness ratio of typical OCTG for collapse applications requires the use of shell elements incorporating shear deformations[15,16]. For the development of the finite element model, the data from the IMS is reconstructed using the first 12 modes of the modal decomposition (**Fig. 8**). Basic data of three tests are shown in Table 1. The results of the 3D models are also shown there, and it is evident that the agreement is very high.

Effect of high and low mode shapes. The same models presented in Table 1 where analyzed when the geometry reconstruction is limited to the lower 4 modes. In all the three cases the numerical results are identical.

It can be concluded that the only modes that determine the collapse behavior are the lower ones.

Effect of the mode phase angle. In **Fig. 4** we plotted the amplitude of each mode (Eq. A-14) as a function of its axial position along the sample. However, in any section the full description of the mode shape includes also the phase angle, which is also varying along the sample (the above mentioned models include both components).

In order to investigate the isolated effect of the phase angle, an ideal 7 in. 26 lb/ft 110 ksi yield stress casing is modeled. Minimum yield, nominal (constant) wall thickness and 0.3% ovality (mode 2) are considered. Four values of the phase angle of the mode 2 are analyzed: 0º, 90º, 180º and 360º (this angle describes the rotation of the main axis in the sample length: 1960mm). In Table 2 we show the calculated collapse pressure normalized with the collapse pressure without twisting (0º). It is evident that the increase of twist results in a higher collapse pressure, for a given value of ovality. **Fig. 9** shows the distribution of axial stresses (on the external surface) at impending collapse.

Effect of connections on collapse resistance

Connections introduce discontinuities along a pipe, hence its effect on the collapse resistance must be considered. Typical OCTG connection analyses are performed on bidimensional axisymmetric models[20], which cannot reproduce the (non axisymmetric) buckling pipes. At the full scale laboratory a special sample was prepared so as to prevent the collapse in the pipe body. A premium connection was machined in the pin and box and the assembly was collapse tested. The final failure shape followed a non axisymmetric pattern, however evidence of plastic failure was observed in the torque shoulder area.

A bidimensional finite element model of the same connection was analyzed. The critical load from the model (10900psi) was essentially the same as the experimental one (10800psi). **Fig. 10** shows the distribution of equivalent plastic strains from the FEA model at impending failure. Plastification of the pin nose and torque shoulder areas is evident. The shearing at the torque shoulder coincides with the observed one, suggesting that the bidimensional model could give accurate results when estimating the external pressure capability of a connection.

An extensive analysis was performed on a typical 7 in. premium connection, with different D/t and material properties. It was found that at low D/t ratios and high grades (typical of collapse situations), API collapse values could be guaranteed, but special precautions should be taken when higher collapse values must be attained.

Conclusions

The results obtained with the combined experimental and numerical procedures presented in this paper contribute to form the basis on which OCTG product engineers design their specifications for high collapse casings. Process control procedures are improved accordingly. The scope of this research is now being extended to include the important cases of axial and bending loads.

Acknowledgements

We acknowledge the financial support for this research of DALMINE (Bergamo, Italy), SIDERCA (Campana, Argentina) and TAMSA (Veracruz, Mexico).

Nomenclature

O_v = ovality, N, dimensionless

ε = eccentricity, N, dimensionless
σ_R = residual stress, m/(L t^2), Pa
σ_Y = yield stress, m/(L t^2), Pa
D = outside diameter, L, mm
L = sample length (under pressure), L, mm
p_{col} = collapse pressure (test), m/(L t^2), Pa
p_{FEA} = collapse pressure (model), m/(L t^2), Pa
t = sample thickness, L, mm
r = radial distance, L, mm
z = axial position, L, mm
q = total turns (decimal)
θ = angle, radians
ω = twist angle, degrees
R_o = best fit radius, L, mm
x_o, y_o = best fit center, L, mm
a_j, b_j = Fourier transform coefficients (mode j), L, mm
A_j = Fourier transform amplitude (mode j), L, mm

References

1. Timoshenko, S.P. and Gere. J.M.: *Theory of Elastic Stability*, Mc Graw Hill Kogakusha, Tokyo (1961).
2. Brush, D.O. and Almroth, B.O., *Buckling of Bars, Plates and Shells*, Mc Graw Hill, New York (1975).
3. Heise, O. and Esztergar, E.P.: "Elastoplastic collapse under external pressure", *ASME, J. Engng. for Industry* (1970) 92, 735.
4. Clinedinst, W.O.: "Analysis of collapse test data and development of new collapse resistance formulas", Report to the API Task Group on Performance Properties (October 1977).
5. Tamita, Y. and Shindo, A.: "On the bifurcation and post bifurcation behavior of thick circular elastic-plastic pipes under lateral pressure", *Comput. Methods Appl. Mech. Engrg*. (1982) 35, 207.
6. Fowler, J.R., Klementich, E.F. and Chappell, J.F.: "Analysis and testing of factors affecting collapse performance of casing", *ASME, J. Energy Res. Tech*., (1983) 105, 574.
7. Krug, G.: "Testing of casing under extreme loads", Institut of Petroleum Engineering, Technische Universität Clausthal (1983).
8. Kanda, M. et al.: "Development of NT-series oil-country tubular good", Nippon Steel Technical Report (1983) 21, 247.
9. Mimura, H., Tamano, T. and Mimaki, T.: "Finite element analysis of collapse strengh of casing", *Nippon Steel Technical Report* (1987) 34, 62.
10. Yeh, M.K. and S. Kyriakides, S.: "Collapse of deepwater pipelines", *ASME, J. Energy Res. Tech.* (1988) 110, 1.
11. Arbocz, J. and Babcock, C.D.: "The effect of general imperfections on the buckling of cylindrical shell", *ASME, J. Appl. Mech.* (1969) 36, 28.
12. Arbocz, J. and Williams, J.G.: "Imperfection surveys of a 10-ft diameter shell structure", *AIAA Journal* (1977) 15, 949.
13. *Bull. 5C3, Bulletin on Formulas and Calculations for Casing, Tubing, Drill Pipe, and Line Pipe Properties*, sixth edition, API (1994).
14. Assanelli, A.P., Toscano, R.G. and Dvorkin E.N.: "Analysis of the collapse of steel tubes under external pressure", *Computational Mechanics, new trends and applications*, E. Oñate and S. Idelshon, Eds., CIMNE, Barcelona, (1998).
15. Dvorkin, E.N. and Bathe, K.J.: "A continuum mechanics based four-node shell element for general nonlinear analysis", *Engng. Comput*. (1984) 1, 77.
16. Bathe, K.J. and Dvorkin, E.N.: "A formulation of general shell elements - The use of mixed interpolation of tensorial components", *Int. J. Numer. Methods in Engng.* (1986) 22, 697.
17. Dvorkin, E.N. and Vassolo, S.I.:"A quadrilateral 2-D finite element based on mixed interpolation of tensorial components", *Engng. Comput*. (1989) 6, 217.
18. Dvorkin, E.N. and Assanelli, A.P.: "Elasto-plastic analysis using a quadrilateral 2-D element based on mixed interpolation of tensorial components", *Proc.* Second International Conference on Computational Plasticity (COMPLAS II), Pineridge Press, Swansea (1989).
19. Dvorkin, E.N., Assanelli, A.P. and Toscano, R.G.: "Performance of the QMITC element in two-dimensional elasto-plastic analyses", *Comput. & Struct.* (1996) 58, 1099.
20. Assanelli, A.P. and Dvorkin E.N.: "Selection of an adequate finite element formulation for modeling OCTG connections", *Computational Mechanics, new trends and applications*, E. Oñate and S. Idelshon, Eds., CIMNE, Barcelona, (1998).
21. Bathe, K.J.: *Finite Element Procedures*, Prentice Hall, Upper Saddle River, New Jersey (1996).
22. Press et al.: *Numerical Recipes*, Cambridge University Press, Cambridge (1986).
23. Shunmugam, M.S.: "Criteria for computer-aided form evaluation", *ASME, J. Engng. for Industry* (1991) 113, 233.
24. Brigham, E.O.: *The fast fourier transform and its applications*, Prentice Hall, Englewood Cliffs, New Jersey (1988).

Appendix A—Algorithm to process the data acquired with the imperfections measuring system

The data is acquired along a spiral path; however, in subsequent analyses we will consider that the points corresponding to a turn are located on a planar section, at an axial distance z_k from an arbitrary origin. As the pitch of the spiral is less than half of the typical wall thickness under analysis, this assumption is valid for the purpose of modelling the collapse test.

The data is fitted to a perfect circle (of unknown center and radius) through a least squares method[10]. This approach is consistent with the subsequent Fourier decomposition.

Input data

r_j: radial distance from the rotation axis to the external surface (see **Fig. 3**), j-th data point.

q_j: total turns corresponding to the j-th data point, measured from an arbitrary defined zero.

Algorithm

1. Initial data reduction

We can define:

$$k = \text{int}\,(q_j) \quad \text{(A-1)}$$

the k-th turn. For this turn we have

$$z_k = \Delta z \cdot \text{int}\,(q_j) \quad \text{(A-2)}$$

$$\theta_i^k = 2\,\pi\,(q_j - \text{int}(q_j)) \quad \text{(A-3)}$$

$$r_i^k = r_j \quad \text{(A-4)}$$

where i=1 for the first j which satisfies $(q_j - \text{int}(q_j)) > 0$ (indication of a new turn). The number of data points per turn

is not constant.

2. Fit to best circle

For the *k*-th section we can define a "*best-fit circle*", with radius R_o and with its center located at (x_o ,y_o) in a Cartesian system, contained in the section plane and with its origin at the section rotation center[10]. The superindex *k* in θ_i^k and r_i^k is omitted. For determining R_o, x_o and y_o we solve the following minimization problem:

$$(R_o, x_o, y_o) = \arg [\ \min E_2(R_o, x_o, y_o)]. \quad \text{(A-5)}$$

$$E_2 = \Sigma_i [r_i - g(\theta_i, R_o, x_o, y_o)]^2. \quad \text{(A-6)}$$

$$g(\theta_i, R_o, x_o, y_o) = [x_o \cos\theta_i + y_o \sin\theta_i] + \text{sqrt}[R_o^2 - (x_o \sin\theta_i - y_o \cos\theta_i)^2]. \quad \text{(A-7)}$$

To solve the above nonlinear minimization problem we apply the Levemberg-Marquard method[22], using as first trial a simplified (linearized) solution in which the expression for *g* reduces to[23]:

$$g_{lin}(\theta_i, R_o, x_o, y_o) = [x_o \cos\theta_i + y_o \sin\theta_i] + R_o. \quad \text{(A-8)}$$

3. Data reduction to new center

Once the center of the "best-fit circle" is determined we reduce the acquired data to it,

$$\hat{x}_i = r_i \cos\theta_i - x_o \quad ; \quad \hat{y}_i = r_i \sin\theta_i - y_o \quad \text{(A-9)}$$

$$\hat{r}_i = \sqrt{\hat{x}_i^2 + \hat{y}_i^2} \quad ; \quad \hat{\theta}_i = \tan^{-1}(\hat{y}_i / \hat{x}_i) \quad \text{(A-10)}$$

4. Fourier transform

We expand using a discrete Fourier transform

$$\hat{a}_j = \frac{1}{\pi} \sum_{k=1}^{M} \left[\hat{r}_k \cos\left(j\hat{\theta}_k \right) \Delta\hat{\theta}_k \right] \quad \text{(A-11)}$$

$$\hat{b}_j = \frac{1}{\pi} \sum_{k=1}^{M} \left[\hat{r}_k \sin\left(j\hat{\theta}_k \right) \Delta\hat{\theta}_k \right] \quad \text{(A-12)}$$

where *M* is the number of samples taken in each turn (360 on average).

$$\hat{r}(\theta) = R_o + \sum_{j=1}^{N} \left[\hat{a}_j \cos(j\theta) + \hat{b}_j \sin(j\theta) \right] \quad \text{(A-13)}$$

where *N* limits the number of modes in the reconstruction of the shape. Sampling theorems[24] put a limit on the maximum value of *N* that can be used (in our case $N<180$). However, for practical applications in collapse calculations, *N* is typically lower than 20.

For practical purposes we define the amplitude of the *j* mode of the Fourier decomposition as:

$$A_j = \sqrt{\hat{a}_j^2 + \hat{b}_j^2} \quad \text{(A-14)}$$

Appendix B—Finite Element Reliability Criteria

CRITERION #1, Basic reliability requirements[16]

- The element formulation must not incorporate numerically adjusted factors.
- The element formulation must not contain spurious rigid body modes.
- The element formulation must satisfy Irons' Patch test.
- The predictive capability of the element must be relatively insensitive to element distortions and changes in material properties (e.g. the formulation must not present incompressible locking)

CRITERION #2, Convergence properties in bending dominated problems. It is important to use finite element formulations of the highest possible predictive capability. Therefore with the same computational effort better results can be obtained, e.g. the element has to be able to represent a state of constant bending.

CRITERION #3, Small/large strain capability. Even though, in standard analyses of OCTG collapse only infinitesimal strains need to be considered, some specific analyses may require the use of a finite strain elasto-plastic analysis capability, hence it is important to select a finite element formulation that is also available for this analyses[18].

CRITERION # 4, Model assessment. It is important to qualify the ability of the finite element formulation to model OCTG collapse performance by comparing its results for some test cases against determinations performed in full scale tests.

SI Metric Conversion Factors

psi	x 6.894 757	E + 00	= kPa
in.	x 2.54*	E + 00	= cm
ksi	x 6.894 757	E + 03	= kPa
lb	x 4.448 222	E + 00	= N
ft	x 3.048*	E - 01	= m

*Conversion factor is exact.

TABLE 1—3D MODEL RESULTS

Sample	*D/t*	σ_Y [ksi]	σ_R/σ_Y	p_{col}/p_{FEA}
1	16.7	122.5	0.17	1.005
2	22.7	114.8	0.38	1.017
3	19.6	120.4	0.27	0.984

Table 2—EFFECT OF THE PHASE ANGLE

ω	$p_{FEA}^{w}/p_{FEA}^{o^\circ}$
90º	1.01
180º	1.05
360º	1.18

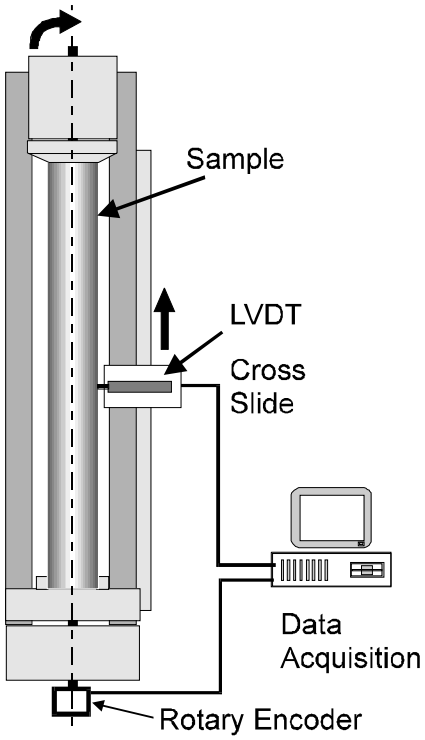

Fig. 1—Layout of imperfections measuring system

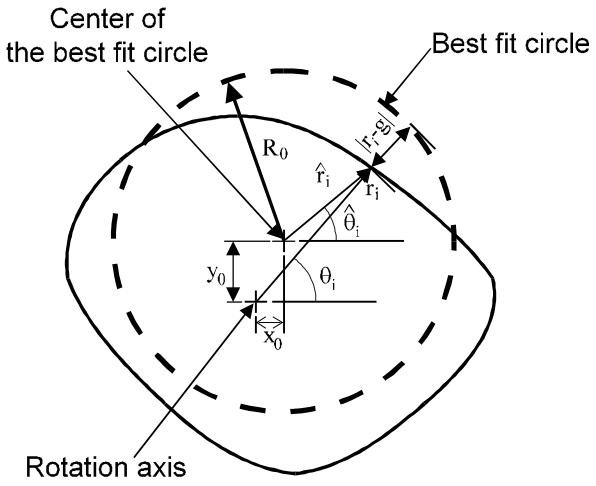

Fig. 2—Data reduction to ideal circle

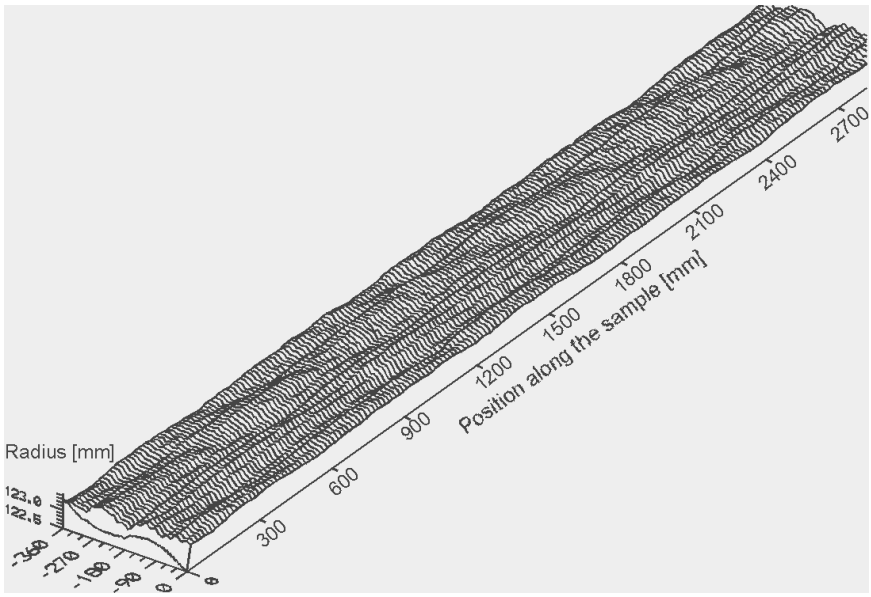

Fig. 3—Mapping of the external surface

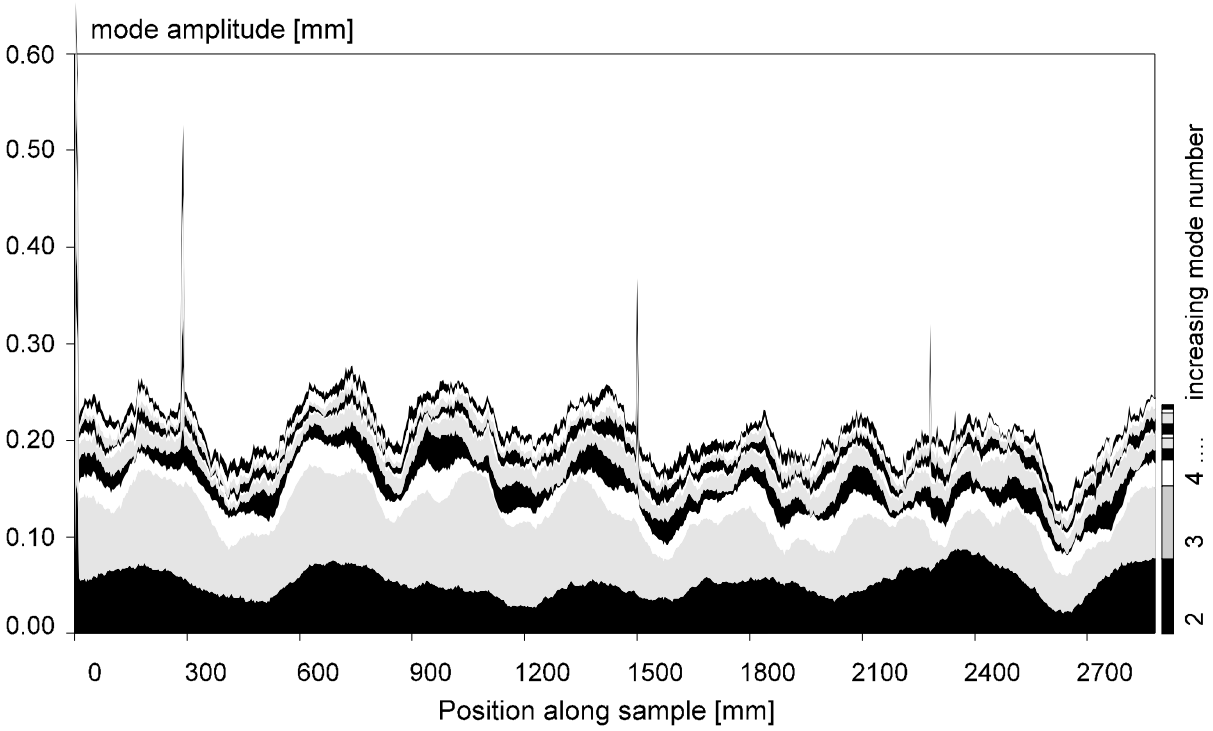

Fig. 4—Modal analysis. Mode amplitude distribution along a sample

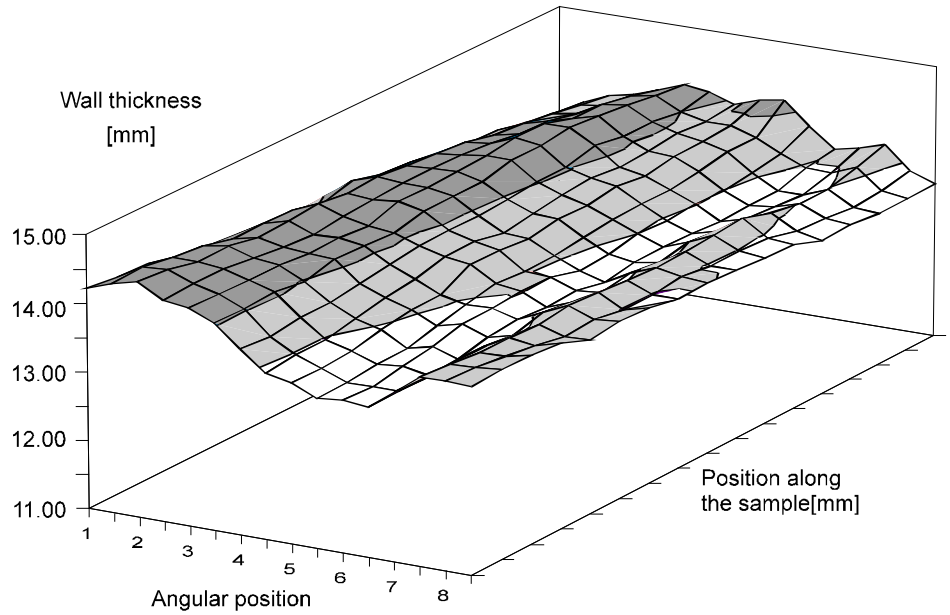

Fig. 5—Wall thickness distribution

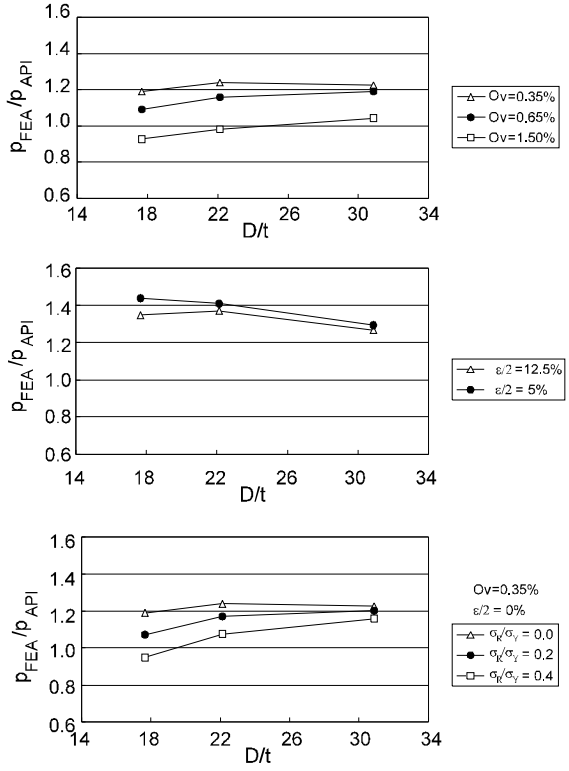

Fig. 6—Parametric study on bidimensional finite element models

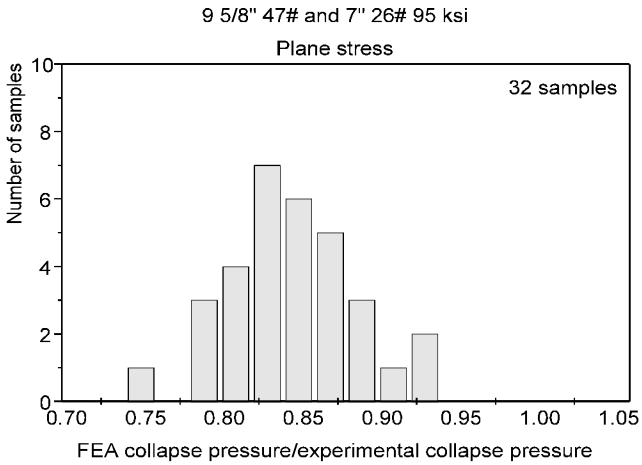

Fig. 7—Comparison between bidimensional models and experimental results

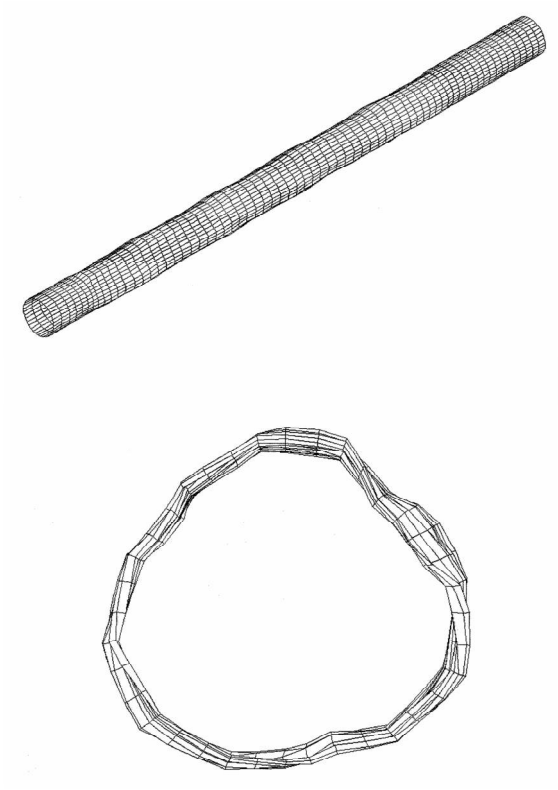

Fig. 8—Three dimensional finite element model (imperfections amplified 50 x)

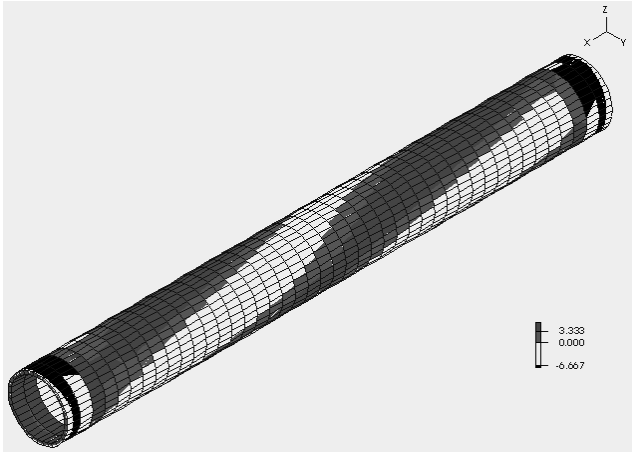

Fig. 9—Finite element model of a pipe with helical ovality. Distribution of axial stresses at the external surface

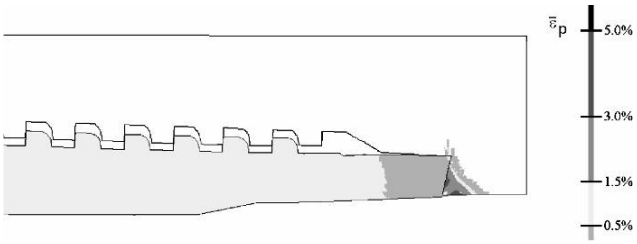

Fig. 10—Plastic collapse of the pin nose of a typical metal to metal seal connection. Distribution of accumulated plastic strains at impending collapse.